AGU PUBLICATIONS

Geophysical Research Letters

RESEARCH LETTER
10.1002/2015GL064908

Key Points:
- As a mushy zone melts from above, convection changes the density profile
- Such melting also produces changes to the solid microstructure
- Melting from above may cause lateral variations in inner core

Correspondence to:
M. I. Bergman,
bergman@SIMONS-ROCK.EDU

Citation:
Yu, J., M. I. Bergman, L. Huguet, and T. Alboussiere (2015), Partial melting of a Pb-Sn mushy layer due to heating from above, and implications for regional melting of Earth's directionally solidified inner core, *Geophys. Res. Lett.*, *42*, 7046–7053, doi:10.1002/2015GL064908.

Received 15 JUN 2015
Accepted 31 JUL 2015
Accepted article online 3 AUG 2015
Published online 10 SEP 2015

Partial melting of a Pb-Sn mushy layer due to heating from above, and implications for regional melting of Earth's directionally solidified inner core

James Yu[1], Michael I. Bergman[1,2], Ludovic Huguet[2], and Thierry Alboussiere[2]

[1]Physics Department, Simon's Rock of Bard College, Great Barrington, Massachusetts, USA, [2]Laboratoire de Geologie de Lyon, Université Lyon 1, ENS de Lyon, CNRS, Villeurbanne, France

Abstract Superimposed on the radial solidification of Earth's inner core may be hemispherical and/or regional patches of melting at the inner-outer core boundary. Little work has been carried out on partial melting of a dendritic mushy layer due to heating from above. Here we study directional solidification, annealing, and partial melting from above of Pb-rich Sn alloy ingots. We find that partial melting from above results in convection in the mushy layer, with dense, melted Pb sinking and resolidifying at a lower height, yielding a different density profile than for those ingots that are just directionally solidified, irrespective of annealing. Partial melting from above causes a greater density deeper down and a corresponding steeper density decrease nearer the top. There is also a change in microstructure. These observations may be in accordance with inferences of east-west and perhaps smaller-scale variations in seismic properties near the top of the inner core.

1. Introduction

In spite of the small cooling rate of Earth's inner core (IC), the small temperature gradient in the core favors the morphological instability [*Mullins and Sekerka* 1964] of the IC boundary [*Loper and Roberts* 1981; *Shimizu et al*. 2005; *Deguen et al*. 2007; *Alexandrov and Malygin* 2011]. This results in dendritic growth of the Fe-rich IC, with a small liquid fraction possibly extending to its center [*Fearn et al*. 1981]. The resulting solidification texturing has been suggested as a possible cause [*Bergman* 1997] for IC elastic and attenuation anisotropy [*Poupinet et al*. 1983; *Morelli et al*. 1986; *Woodhouse et al*. 1986; *Creager* 1992; *Souriau and Romanowicz* 1996]. In addition, seismology has also inferred east-west variations in IC elastic anisotropy [*Tanaka and Hamaguchi* 1997], attenuation anisotropy [e.g., *Cao and Romanowicz* 2004], and isotropic velocity [*Tanaka and Hamaguchi* 1997; *Niu and Wen* 2001]. More recently, *Cormier and Attanayake* [2013], *Iritani et al*. [2014], and *Yee et al*. [2014] argue for smaller-scale variations in seismic properties.

Moreover, seismology has suggested a dense, i.e., Fe-rich, layer at the base of the outer core (OC) [*Souriau and Poupinet* 1991]. The cause of this layer could be IC translation [*Alboussiere et al*. 2010; *Monnereau et al*. 2010], which would result in melting at the inner-outer core boundary of one hemisphere. As the IC translates, the microstructure may evolve, either through diffusion or recrystallization [*Bergman et al*. 2010; *Al-Khatatbeh et al*. 2013], because the solidification microstructure is not necessarily thermodynamically stable once the solidification ceases [*Marsh and Glicksman* 1996]. These processes that lower surface free energy (or energy due to defects as a result of deformation) are known as annealing and occur more rapidly at high temperature. They can result in a weakening of an existing (e.g., solidification) texture and could be a cause for hemispherical variations in elastic anisotropy [*Bergman et al*. 2010]. Moreover, grain growth during translation and annealing might result in east-west variations in attenuation and isotropic velocity [*Monnereau et al*. 2010].

Alternatively, *Sumita and Olson* [1999] and *Aubert et al*. [2008] have suggested that mantle control over OC convection might be the cause for east-west and regional seismic variations. *Gubbins et al*. [2011] further suggested that such mantle control could even result in regional melting of the IC boundary, resulting in the Fe-rich layer at the base of the OC. Translation on its own cannot explain a complex pattern of IC seismic properties, but *Mizzon and Monnereau* [2013] find that for an IC viscosity of about 10^{18} Pa s IC convection (resulting in shear) and translation can coexist, in agreement with results by *Deguen* [2012].

In this study we examine experimentally the processes of directional solidification, annealing, and partial melting from above of a Pb-rich Sn alloy in order to simulate these processes in Earth's IC. In particular we

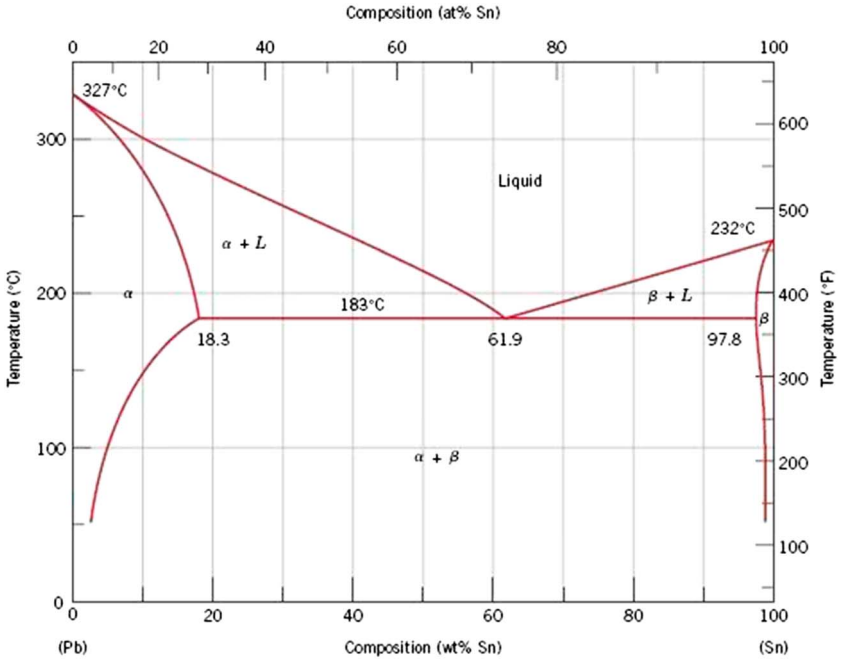

Figure 1. Pb-Sn phase diagram.

are interested in changes in both the alloy's microstructure, due to diffusion, and the resulting density profile, due to interdendritic liquid convection.

Several related studies have been carried out. *Hallworth et al.* [2004] studied melting from above of a self-supporting matrix of solid KNO_3 crystals bathed in an aqueous KNO_3 solution that also contains some proportion of inert glass beads. They found that the melting from above can result in solidification below due to liquid convection as the denser KNO_3 sinks. Their study was focused on understanding postdepositional, prelithification mechanisms to induce compositional layering in sedimentary and igneous rocks and was therefore not concerned with a dendritic microstructure. *Hallworth et al.* [2005], *Butler et al.* [2006], and *Butler* [2011] analytically and numerically studied the KNO_3 system, finding that the heat from above is used in the dissolution of solid crystals at the top of the layer, resulting in mass redistribution through brief but intense convection, as suggested in the experiments.

2. Experimental Procedure

We used a Pb-25 wt % Sn alloy because it forms a simple eutectic system (Figure 1) with low pure-metal melting temperatures and because there is a large density difference between Pb and Sn. We work on the Pb side of the eutectic, resulting in Pb-rich dendrites, although there is some solubility of Sn in the solid Pb phase, and vice versa. Although Pb is cubic whereas Fe under IC conditions is likely hexagonal close packed (hcp) [*Tateno et al.* 2010; *Lincot et al.* 2015], the occurrence of dendrites does not depend on the crystal structure [*Hellawell and Herbert* 1962], though the crystallographic direction and form of the dendrites does, with cubic dendrites being more nearly figures of revolution and hcp dendrites taking on the form of platelets parallel to the basal plane.

Figure 2 is a sketch of our furnace. We first melt 1800 g of Pb-25 wt % Sn (1350 g of 99.9% pure Pb and 450 g of 99.9% pure Sn) in a cylindrical graphite crucible that slides down into a resistance furnace (maximum power 840 W), with the heating coils located near the top of the crucible and cooling tubes machined into the furnace's base through which we circulate water. The furnace sidewalls are thermally insulated. Two bores in the walls of the crucible hold type K thermocouples at heights of 3 mm and 153 mm. For the solidification experiments we use the lower thermocouple (labeled 1 in Figure 2) as the feedback thermocouple for a programmable thermal controller, while the upper thermocouple (labeled 2) is passive. We ran experiments at two different temperature gradients depending on the presence of an insulating spacer between the crucible bottom and the cooling tubes.

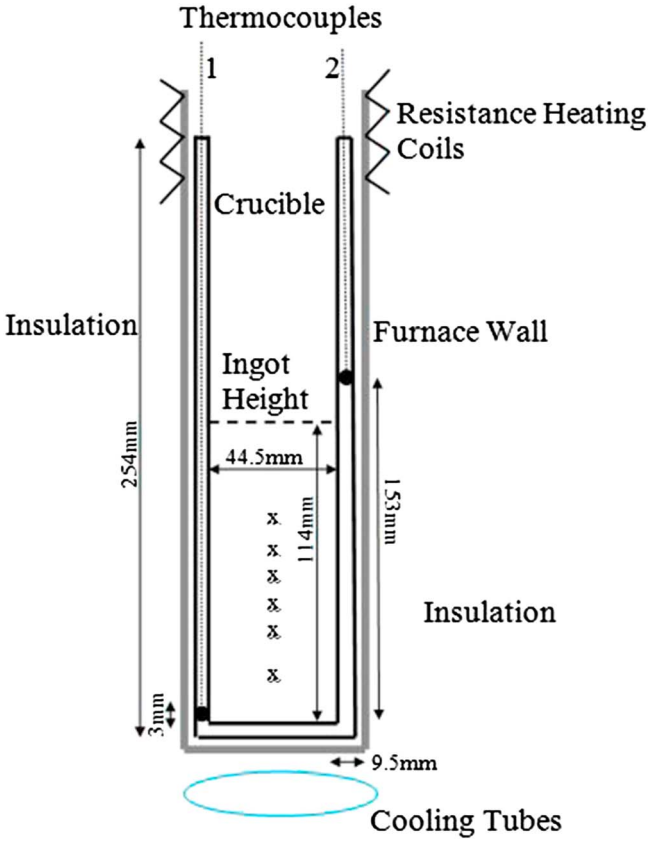

Figure 2. Sketch of the directional solidification furnace. The crosses are the rough locations of the ingot section centers for which we computed the density.

Once the lower (cooler) thermocouple is at 350°C and the alloy is molten, we program cool the alloy at a rate of .25° C/min down to room temperature. At this time, the larger temperature gradient is about 1.3°C/mm and the smaller .7°C/mm (the gradients may not be constant, but they are based on just the two thermocouple positions). Because of the fixed nature of the furnace, these temperature gradients necessarily decrease as the overall temperature decreases. This cooling rate and these temperature gradients are in the range for upward directional solidification to produce dendritic growth (Figure 3a). The resulting ingots have a height of 114 mm. This first step of our experiments simulates directional solidification of Earth's IC.

The second step is meant to simulate annealing (perhaps due to translation), which is essentially exposure to high temperature without deformation. We carry out this step by removing a cooled, directionally solidified ingot and placing it in an isothermal oven at a temperature of 170°C, just beneath the Pb-Sn eutectic temperature, for 1 week. We then let it cool at room temperature, which took a couple of hours. Based on the diffusivity of Pb close to its melting temperature ($D = 4.5 \times 10^{-14}\,m^2/s$ [*Porter and Easterling*, 1992]) and the length scale of secondary dendrites, i.e., side-branches, seen in Figure 3a ($L = 50$–$100\ \mu m$), we determined that 1 week is sufficient time $\tau = L^2/D$ for significant coarsening. This is borne out in Figure 3b. In some experiments we skipped the annealing step and proceeded directly from directional solidification to partial melting from above.

The third step, partial melting from above, is meant to simulate regional melting of the IC boundary. To accomplish this, we put an annealed ingot (or a directionally solidified one if we skipped the annealing step)

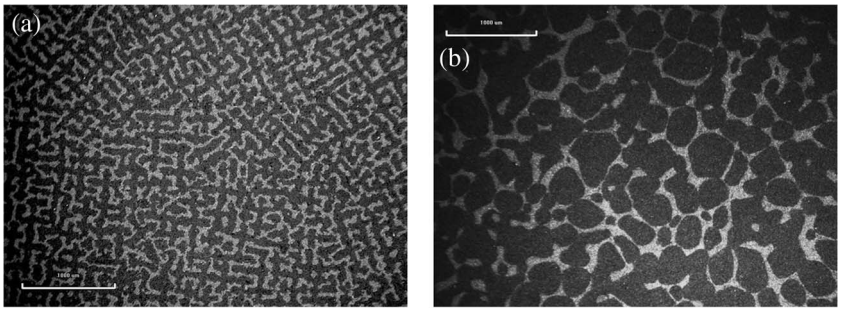

Figure 3. Micrographs of horizontal slices at a height of 63 mm, 40X magnification (the bars in all micrographs are 1 mm), polished to 3 μm, and etched with 2% nital for 30 s. The Pb-rich phase is dark, the eutectic phase light. (a) A directionally solidified ingot with the smaller temperature gradient, showing cross-shaped, Pb-rich dendrites. (b) A directionally solidified (with the smaller temperature gradient) and then annealed ingot, showing coarsening as the secondary arms have become more globular.

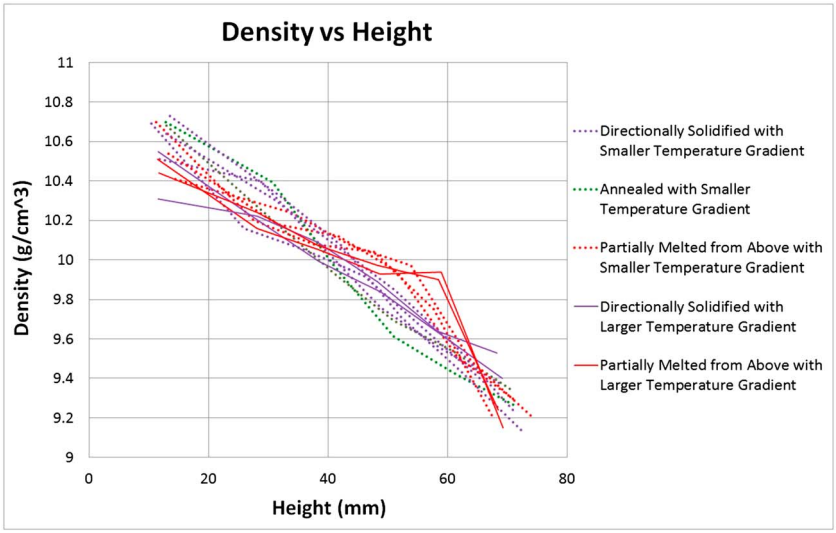

Figure 4. Plot of density versus height for ingots after each of the three processes, for two temperature gradients. We skipped the annealing step for the larger temperature gradient. The key observation here is that the ingots partially melted from above have densities that differ maximally from those only directionally solidified/annealed at a height of 55 mm (smaller temperature gradient, dotted red lines) and at 60 mm (larger temperature gradient, solid red lines). Mass must be conserved, and above these heights the ingots partially melted from above have densities that decrease more rapidly with height.

back in the crucible and furnace. Here for the partial melting from above experiments, we use the upper thermocouple (labeled 2 in Figure 2) as the feedback thermocouple. We set the temperature at thermocouple 2 to be 250°C, with either the smaller or larger temperature gradient. These temperature profiles cross the liquidus temperature at some height in the ingot, as discussed in section 3. We exposed an ingot to one of these temperature profiles for 4 h, before turning off the furnace and cooling to room temperature.

After each of the three steps, we machined horizontally 10.0 mm thick slices for some of the ingots and determined their densities. Some of these slices we also polished using standard metallographic techniques in order to obtain micrographs. We did the same for a few vertically cut slices.

3. Results

Figure 4 plots density versus height for a number of ingots after each of the three steps, for the two temperature gradients. The horizontal cuts produce five 10.0 mm thick slices, plus the bottom and top pieces, which are thicker. We plot the densities at the midpoints of each section, also accounting for machining losses.

Figure 4 shows that the directionally solidified ingots (purple) and the annealed ingots (green) do not show a great difference in their density profiles. Although the annealing coarsens the microstructure via diffusion (Figure 3b), there is unsurprisingly not a change in the macrosegregation of the alloying elements since the annealing temperature was below the eutectic temperature. However, the ingots partially melted from above (red) show a consistently different trend, with a density difference peaking at a height of about 55 mm (for the smaller temperature gradient, dotted line) and about 60 mm (for the larger temperature gradient, solid line). Above about 65 mm the densities of those ingots partially melted from above drop more steeply than those ingots that were only directionally solidified/annealed. Below about 45 mm the densities of those ingots partially melted from above differ little from the others. Since the ingots partially melted from above have maximal density differences near 55 and 60 mm, to conserve mass, it is consistent that they have correspondingly lower densities at greater heights.

Our hypothesis is that as dense, Pb-rich dendrites melt from above, the resulting liquid sinks and then resolidifies at a greater depth where it is cooler as was observed in *Hallworth et al*. [2004]. Obviously, melted interdendritic Sn-rich liquid must then rise, which is apparent in Figure 5a with the presence of more lighter-colored eutectic above 58 mm. This vertical section is cut from a height in the ingot where the actual crucible

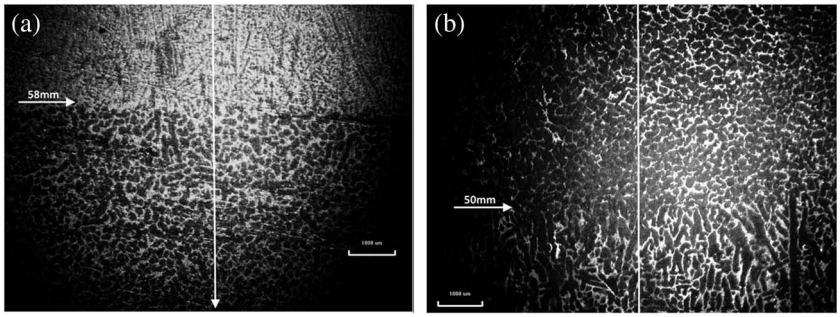

Figure 5. Micrographs of vertical slices at two different heights of an ingot partially melted from above (directionally solidified with the smaller temperature gradient and without the annealing step), 20X magnification (the bars in all micrographs are 1 mm), polished to 3 μm, and etched with 2% nital for 25 s. The Pb-rich phase is dark, the eutectic phase light. The vertical lines denote the vertical direction in the slices. (a) The horizontal front at 58 mm (marked with arrow) is likely due to complete melting and dendritic resolidification above and coarsening below (in a region that was partially melted). (b) The horizontal front at 50 mm (marked with arrow) is likely due to coarsening above (in a region that was partially melted), with the original vertical dendrites of the directional solidification microstructure preserved below (though in a region that was also partially melted). The lower edge of Figure 5a and the upper edge of Figure 5b are contiguous.

temperature crossed the liquidus (see following paragraphs and Figure 6). Above this crossover, melting was complete, and below, melting was partial to the eutectic phase and some Pb-rich dendrites. The density of this section (dotted red) is comparable to those only directionally solidified/annealed, presumably because the greater fraction of lower density eutectic phase above 58 mm is balanced by the higher density below.

To confirm the cause of the mass redistribution, we calculated the mass fraction of Pb/Sn (assuming linear mixing) from the density of each directionally solidified slice in Figure 4. From the phase diagram, Figure 1, we then computed the liquidus temperatures of those compositions versus height. We plot these in Figure 6, along with the two actual crucible temperature profiles. For the smaller temperature gradient this profile is based on just the two thermocouple measurements, but for the larger temperature gradient we took measurements approximately every 10 mm by manually raising the thermocouple. According to Figure 6, above about 60 mm the actual crucible temperature is greater than the liquidus, so there should have been complete melting above this height. Below this height, eutectic phase and outer layers of Pb-rich dendrites would have melted in accordance with the phase diagram, Figure 1.

This is consistent with the horizontal front seen at about 58 mm in Figure 5a, which is the line above which there was complete melting, with resolidification occurring with a dendritic microstructure. At the end of the experiment we simply turned off all heating, so the crucible cooled much more quickly than during a

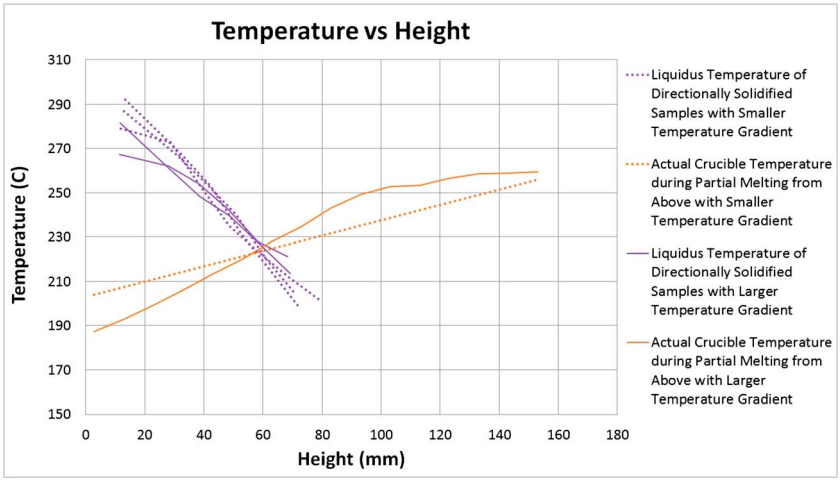

Figure 6. Plot of liquidus temperatures and crucible temperatures during partial melting from above versus height, for two temperature gradients.

programmed directional solidification, resulting in the observed finer microstructure. Below this line melting was incomplete and the remaining dendritic structure appeared to have coarsened (with loss of secondary arms) during the partial melting from above. This height coincides with where the density profiles of the ingots partially melted from above differ maximally from those only directionally solidified/annealed (about 55 mm, Figure 4). We believe that this correspondence results from the pooling of dense Pb-rich melt in the top of the partially melted zone where the permeability is still relatively high. We will discuss this further in the next section.

Interestingly, at a height of about 50 mm we find another front, below which the original directional solidification microstructure is more apparent (Figure 5b). Figure 4 shows there was little mass redistribution below this line. However, it is not clear why this front should be so sharp since according to Figure 6, the entire ingot heights were above the eutectic temperature during partial melting from above, and coarsening is a diffusive phenomenon. Vertical sections of the original directional solidification microstructure show no such fronts.

4. Discussion and Geophysical Implications

If the IC is translating [*Alboussiere et al*. 2010; *Monnereau et al*. 2010] or lateral variations in heat flow from the OC are sufficiently large [*Gubbins et al*. 2011], then the IC is regionally melting even as it overall directionally solidifies. Those regions that are solidifying are likely taking on a dendritic microstructure [*Loper and Roberts* 1981; *Shimizu et al*. 2005; *Deguen et al*. 2007; *Alexandrov and Malygin* 2011], and if the IC is translating without deformation, it is likely annealing [*Bergman et al*. 2010; *Al-Khatatbeh et al*. 2013] before melting from above. Directional solidification has been well studied, as has annealing, though perhaps not as much in the context of Earth's IC. Here we study partial melting from above.

The first work to study melting of a mushy layer was a theoretical one by *Feltham and Worster* [2000]. Although they studied the evolution of the solid fraction, which is related to our measurements of density profiles, they did not consider convection driven by the melting in the mushy layer. As a result, their similarity solutions do not admit the possibility of macrosegregation resulting from the melting, and hence general changes to the shape of the density and solid fraction profiles. *Hallworth et al*. [2004] seem to be the first to observe that melting from above of a reactive mixed phase region can result in solidification deeper within that region as a result of convection, which was supported with theoretical work by *Hallworth et al*. [2005], *Butler et al*. [2006], and *Butler* [2011], but these studies were for a porous mixed phase region that was not originally formed by directional solidification, as is the case here and in Earth's core.

As can be seen in Figure 3b, annealing produces coarser dendrites with less sidebranching, as a result of diffusion. This is in accordance with *Marsh and Glicksman* [1996] and *Al-Khatatbeh et al*. [2013]. As expected, Figure 4 shows that annealing does not change the directional solidification density profile, but surprisingly, ingots that were first annealed before partial melting from above have similar density profiles to those that skipped the annealing step (in Figure 4, two of the red dotted lines skipped the annealing steps, one did not, but they are all similar). This seems surprising because one might expect the sidebranches of the directional solidification microstructure (Figure 3a) to inhibit convection more effectively than the less tortured annealed microstructure (Figure 3b).

A useful measure of convection in a mushy zone is the mushy zone Rayleigh number Ra_m [*Fowler* 1985; *Worster* 1991]. $Ra_m = \beta^* |\Delta C| g \Pi L / \nu\kappa$, where $\beta^* = \beta - \Gamma\alpha$ and β and α are the coefficients of solute and thermal expansion. Assuming a linear liquidus Γ, $\Gamma\Delta C = \Delta T$, where $\Delta C = C_o - C_e$ and $\Delta T = T_L(C_o) - T_e$. Here C_o is the initial percent melt composition, 25; $T_L(C_o)$ is the liquidus temperature at this composition, 270°C; and C_e and T_e are the eutectic composition and temperature, 62 and 183°C, so that $|\Delta C| = 37$; g is gravity, and ν and κ are the fluid viscosity and thermal diffusivity. Values for α, β, Γ, ν, and κ can be found in Table II of *Bergman et al*. [1997]. L is the thermal length scale, κ/V, where V is the solidification growth rate. $V = (dT/dt)/(dT/dx)$, where dT/dt is the programmed cooling rate, .25°C/min, and dT/dx is the (nonconstant) furnace temperature gradient. Finally, Π is the permeability.

In estimating Π we follow *Bergman et al*. [1997], setting $\Pi = \delta^2$, where δ is the averaged measured interdendritic spacing through which liquid must flow. One might hope that this accounts for both the local liquid fraction and the geometry of the dendritic matrix. For Figure 3a, we made 65 measurements, finding $\delta = 43$ μm, yielding $\Pi = 1.8 \times 10^{-9}$ m^2. Using the initial dT/dx, .7°C/mm, the initial $V = 5.8 \times\times 10^{-3}$ mm/s, increasing as the

temperature gradient decreases as the furnace cools. This yields an initial $Ra_m = 2300$, which is supercritical for convection [*Bergman et al*. 1997], consistent with the macrosegregation in Figure 4. Although at least one ingot exhibited a freckle trail [*Copley et al*. 1970], we did not consistently find evidence for chimneys. However, *Bergman et al*. [1999] found that the absence of chimneys does not affect the macrosegregation, and the directional solidification density profiles found here are similar to those in *Bergman et al*. [1997].

A calculation of Ra_m for Figure 3b yields 2400, which is comparable to that for Figure 3a. This likely explains why the density profiles for the ingots partially melted from above did not depend on whether the directionally solidified ingots were annealed (all the dotted red lines in Figure 4 are similar). Finally, a calculation of Ra_m at a lower height in the same ingot as shown in Figure 3a yields a lower value, 600, which might explain why convection does not effectively extend deeper down during partial melting from above (the density profiles in Figure 4 are all similar below a height of 45 mm). We do not, however, have a good explanation for the sharp front seen in Figure 5b.

The primary observables from these experiments are that the density profiles of the directionally solidified ingots, partially melted from above, differ from those that are only directionally solidified/annealed (Figure 4) and that microstructure changes upon partial melting from above (Figures 5a and 5b). We emphasize that the results of these experiments apply for regional as well as hemispherical melting from above. In the case that the IC is translating eastward [*Alboussiere et al*. 2010] then the top of the eastern IC might be less dense than the corresponding top of the western hemisphere and that deeper down the eastern hemisphere might be more dense than the corresponding depth in the western hemisphere.

Niu and Wen [2001] found that in the uppermost 100 km of the IC the isotropic velocity in the Eastern Hemisphere is .8% faster than that in the Western Hemisphere. The top of the Eastern Hemisphere being faster is consistent with the experimental results if we assume that variations in the compressional velocity $V_P = ((\kappa + 4/3\mu)/\rho)^{1/2}$ are due to variations in density ρ, and the bulk and shear moduli κ and μ are constant. The density contrast between Pb-rich dendrites and eutectic Pb-Sn is 1.8 g/cm^3, whereas that between the top of the IC and base of the OC is only 0.6 g/cm^3 (preliminary reference Earth model [*Dziewonski and Anderson*, 1981]). Scaling the density difference from what we find in Figure 4, we calculate that density differences arising from convection due to melting of the IC could result in a .4% variation in isotropic velocity. This could be an underestimate because it does not take into account the greater convective efficacy due to the larger length scale in the IC.

The depth dependence of the east-west variations in isotropic velocity is still uncertain: *Cao and Romanowicz* [2004] and *Iritani et al*. [2014] find little difference beneath 100–200 km, whereas *Lythgoe et al*. [2014] find variations extending to the center. However, it is likely that the high pressure of the core will squeeze out a high fraction of interdendritic melt beneath a depth of a few kilometers [*Sumita et al*. 1996], so although intriguing, it is not clear whether convection due to melting is viable for explaining the observed depth extent of east-west variations in isotropic velocity. It is also possible that the direction of translation may be westward and that perhaps it is the change in microstructure that plays the key role in determining the heterogeneity of seismic velocity and attenuation. Experiments underway using a centrifuge and the melting from above of directionally solidified NH_4Cl and ultrasonic measurements on the different microstructures may help to answer these questions.

Acknowledgments
Michael Bergman acknowledges support from the U.S. NSF and ENS de Lyon for a visiting fellowship to Lyon. Thierry Alboussiere acknowledges support from the program PNP of INSU. We would like to thank the reviewers for their suggestions to improve the presentation of this work. We present our methods and data in this study, and they are available upon request from the authors.

The Editor thanks Valentin Gischig and an anonymous reviewer for their assistance in evaluating this paper.

References

Alboussiere, T., R. Deguen, and M. Melzani (2010), Melting-induced stratification above the Earth's inner core due to convective translation, *Nature*, *466*, 744–747.

Alexandrov, D. V., and A. P. Malygin (2011), Coupled convective and morphological instability of the inner core boundary of the Earth, *Phys. Earth Planet. Int.*, *189*, 134–141.

Al-Khatatbeh, Y., M. I. Bergman, D. J. Lewis, Z. Mason, L. Zhu, and S. Rosenstock (2013), Annealing of directionally solidified alloys revisited: No loss of solidification texture in Earth's inner core, *Phys. Earth Planet. Int.*, *223*, 32–39.

Aubert, J., H. Amit, G. Hulot, and P. Olson (2008), Thermochemical flows couple the Earth's inner core growth to mantle heterogeneity, *Nature*, *454*, 758–761.

Bergman, M. I. (1997), Measurements of elastic anisotropy due to solidification texturing and the implications for Earth's inner core, *Nature*, *389*, 60–63.

Bergman, M. I., D. R. Fearn, J. Bloxham, and M. C. Shannon (1997), Convection and channel formation in solidifying Pb-Sn alloys, *Metall. Trans. A*, *28*, 859–866.

Bergman, M. I., D. R. Fearn, and J. Bloxham (1999), Suppression of channel convection in solidifying Pb-Sn alloys via an applied magnetic field, *Metall. Trans. A*, *30*, 1809–1815.

Bergman, M. I., D. J. Lewis, I. H. Myint, L. Slivka, S. I. Karato, and A. Abreu (2010), Grain growth and loss of texture during annealing of alloys, and the translation of Earth's inner core, *Geophys. Res. Lett.*, *37*, L22313, doi:10.1029/2010GL045103.
Butler, S. L. (2011), Effective transport rates and transport-induced melting and solidification in mushy layers, *Phys. Fluids*, *23*, 016602, doi:10.1063/1.3541840.
Butler, S. L., H. E. Huppert, and M. G. Worster (2006), Numerical modelling of convection in a reactive porous medium with a mobile mush-liquid interface, *J. Fluid Mech.*, *549*, 99–129.
Cao, A., and B. Romanowicz (2004), Hemispherical transition of seismic attenuation at the top of the Earth's inner core, *Earth Planet. Sci. Lett.*, *228*, 243–253.
Copley, S. M., A. F. Giamei, S. M. Johnson, and M. F. Hornbecker (1970), The origin of freckles in unidirectionally solidified castings, *Metall. Trans. A*, *1*, 2193–2204.
Cormier, V. F., and J. Attanayake (2013), Earth's solid inner core: Seismic implications of freezing and melting, *J. Earth Sci.*, *24*, 683–698.
Creager, K. C. (1992), Anisotropy of the inner core from differential travel times of the phases PKP and PKIKP, *Nature*, *356*, 309–313.
Deguen, R. (2012), Structure and dynamics of Earth's inner core, *Earth Planet. Sci. Lett.*, *333*, 211–225.
Deguen, R., T. Alboussiere, and D. Brito (2007), On the existence and structure of a mush at the inner core boundary of the Earth, *Phys. Earth Planet. Int.*, *164*, 36–49.
Dziewonski, A. M., and D. L. Anderson (1981), Preliminary reference Earth model, *Phys. Earth Planet. Int.*, *25*, 297–356.
Fearn, D. R., D. E. Loper, and P. H. Roberts (1981), Structure of the Earth's inner core, *Nature*, *292*, 232–233.
Feltham, D. L., and M. G. Worster (2000), Similarity solutions describing the melting of a mushy layer, *J. Cryst. Growth*, *208*, 746–756.
Fowler, A. C. (1985), The formation of freckles in binary alloys, *IMA J. Appl. Maths*, *35*, 159–174.
Gubbins, D., B. Sreenivasan, J. Mound, and S. Rost (2011), Melting of the Earth's inner core, *Nature*, *473*, 361–363.
Hallworth, M. A., H. E. Huppert, and A. W. Woods (2004), Crystallization and layering induced by heating a reactive porous medium, *Geophys. Res. Lett.*, *31*, L13605, doi:10.1029/2004GL019950.
Hallworth, M. A., H. E. Huppert, and A. W. Woods (2005), Dissolution-driven convection in a reactive porous medium, *J. Fluid Mech.*, *535*, 255–285.
Hellawell, A., and P. M. Herbert (1962), The development of preferred orientations during the freezing of metals and alloys, *Proc. R. Soc. London A*, *269*, 560–573.
Iritani, R., N. Takeuchi, and H. Kawakatsu (2014), Intricate heterogeneous structures of the top 300 km of the Earth's inner core inferred from global array data: 1. Regional 1D attenuation and velocity profiles, *Phys. Earth Planet. Int.*, *230*, 15–27.
Lincot, A., S. Merkel, and P. Cardin (2015), Is inner core seismic anisotropy a marker for plastic flow of cubic iron?, *Geophys. Res. Lett.*, 1326–1333, doi:10.1002/2014GL062862.
Loper, D. E., and P. H. Roberts (1981), A study of conditions at the inner core boundary of the Earth, *Phys. Earth Planet. Int.*, *24*, 302–307.
Lythgoe, K. H., A. Deuss, J. F. Rudge, and J. A. Neufeld (2014), Earth's inner core: Innermost inner core or hemispherical variations?, *Earth Planet. Sci. Lett.*, *385*, 181–189.
Marsh, S. P., and M. E. Glicksman (1996), Overview of geometric effects on coarsening of mushy zones, *Metall. Trans. A*, *27*, 557–567.
Mizzon, H., and M. Monnereau (2013), Implication of the lopsided growth for the viscosity of Earth's inner core, *Earth Planet. Sci. Lett.*, *361*, 391–401.
Monnereau, M., M. Calvet, L. Margerin, and A. Souriau (2010), Lopsided growth of Earth's inner core, *Science*, *328*, 1014–1017.
Morelli, A., A. M. Dziewonski, and J. H. Woodhouse (1986), Anisotropy of the inner core inferred from PKIKP travel times, *Geophys. Res. Lett.*, *13*, 1545–1548, doi:10.1029/GL013i013p01545.
Mullins, W. W., and R. F. Sekerka (1964), Stability of a planar interface during solidification of a dilute binary alloy, *J. App. Phys.*, *35*, 444–451.
Niu, F., and L. Wen (2001), Hemispherical variations in seismic velocity at the top of the Earth's inner core, *Nature*, *410*, 1081–1084.
Porter, D. A., and K. E. Easterling (1992), *Phase Transformations in Metals and Alloys*, 2nd ed., Chapman & Hall, London.
Poupinet, G., R. Pillet, and A. Souriau (1983), Possible heterogeneity of the Earth's inner core deduced from PKIKP travel times, *Nature*, *305*.
Shimizu, H., J.-P. Poirer, and J.-L. LeMouel (2005), On crystallization at the inner core boundary, *Phys. Earth Planet. Int.*, *151*, 37–51.
Souriau, A., and G. Poupinet (1991), The velocity profile at the base of the liquid core from PKP(BC+Cdiff) data: An argument in favor of radial inhomogeneity, *Geophys. Res. Lett*, *18*, 2023–2026, doi:10.1029/91GL02417.
Souriau, A., and B. Romanowicz (1996), Anisotropy in inner core attenuation: A new type of data to constrain the nature of the solid core, *Geophys. Res. Lett.*, *23*, 1–4, doi:10.1029/95GL03583.
Sumita, I., and P. Olson (1999), A laboratory model for convection in Earth's core driven by a thermally heterogeneous mantle, *Science*, *286*, 1547–1549.
Sumita, I., S. Yoshida, M. Kumazawa, and Y. Hamano (1996), A model for sedimentary compaction of a viscous medium and its application to inner core growth, *Geophys. J. Int.*, *124*, 502–524.
Tanaka, S., and H. Hamaguchi (1997), Degree one heterogeneity and hemispherical variation of anisotropy in the inner core from PKP(BC)-PKP(DF) times, *J. Geophys. Res.*, *102*, 2925–2938, doi:10.1029/96JB03187.
Tateno, S., K. Hirose, Y. Ohishi, and Y. Tatsumi (2010), The structure of iron in Earth's inner core, *Science*, *330*, 359–360.
Yee, T.-G., J. Rhie, and H. Tkalcic (2014), Regionally heterogeneous uppermost inner core observed with Hi-net array, *J. Geophys. Res. Solid Earth*, *119*, 7845–7823, doi:10.1002/2014JB011341.
Woodhouse, J. H., D. Giardini, and X.-D. Li (1986), Evidence for inner core anisotropy from free oscillations, *Geophys. Res. Lett.*, *13*, 1549–1552, doi:10.1029/GL013i013p01549.
Worster, M. G. (1991), Natural convection in a mushy layer, *J. Fluid Mech.*, *224*, 335–359.